Food Hydrocolloids 161 (2025) 110863

Contents lists available at ScienceDirect

Food Hydrocolloids

journal homepage: www.elsevier.com/locate/foodhyd

Amyloid aggregation in mixed whey proteins

Sara Venturi [a], Barbara Rossi [b], Fatima Matroodi [b,c], Renato Torre [a,d], Andrea Lapini [a,e], Paolo Foggi [a,f,g], Alessandro Di Michele [h], Paola Sassi [a,f], Marco Paolantoni [f,**], Sara Catalini [a,g,h,*]

[a] European Laboratory for Non-Linear Spectroscopy, Università di Firenze, Via Nello Carrara 1, 50019, Sesto Fiorentino, Italy
[b] Elettra-Sincrotrone Trieste, S.S. 114 km 163.5, Basovizza, 34149, Trieste, Italy
[c] Department of Physics, Shahid Chamran university of Ahvaz, Ahvaz, Iran
[d] Dipartimento di Fisica ed Astronomia, Università di Firenze, Via G. Sansone, 1, 50019, Sesto Fiorentino, Italy
[e] Dipartimento di Scienze Chimiche, della Vita e della Sostenibilità Ambientale, Università degli Studi di Parma, Parco Area delle Scienze, 17/A, 43124, Parma, PR, Italy
[f] Dipartimento di Chimica, Biologia e Biotecnologie, Università di Perugia, Via Elce di sotto 8, 06123, Perugia, Italy
[g] CNR-INO, Consiglio Nazionale Delle Ricerche – Istituto Nazionale di Ottica, Largo Fermi 6, 50125, Florence, Italy
[h] Dipartimento di Fisica e Geologia, Università di Perugia, 06123 Via Pascoli, Perugia, Italy

ARTICLE INFO

Keywords:
whey proteins aggregation
protein-based hydrogels
β-lactoglobulin
albumin
UV resonance Raman
FTIR
SAXS
HD-TG

ABSTRACT

The fundamental principles behind the complexity of protein assembly, especially in mixed protein systems and crowded environments, remain elusive. This study provides molecular, structural, and viscoelastic insights into the aggregation and gelation processes in aqueous solutions of pure and mixed β-lactoglobulin and albumin whey proteins. To better understand protein aggregation in complex systems, we used a multi-technique approach that spans from molecular to macroscopic length scales. Our results show that, under low pH and heat denaturation, β-lactoglobulin tends to form ordered amyloid-type aggregates, while bovine serum albumin forms non-amyloid aggregates. In crowded environments, all protein solutions tested develop composite gel networks with distinct molecular origins. Here the ability to control the amyloid aggregate content, which has a substantial effect on the structural and viscoelastic properties of these composite gels, has been demonstrated. Gel structure and viscosity are crucial parameters to control for the food industry, as they play a key role in determining the softness and texture of food products.

1. Introduction

Alterations of the physiological environment where proteins maintain their native conformation can induce protein denaturation due to the exposition of specific moieties able to establish intermolecular interactions to form aggregates (Catalini et al., 2021, 2022, pp. 183–225; Dobson, 2004). Understanding and controlling the molecular steps of aggregation in view of the development of soft materials with specific properties is an exceptionally challenging task, especially in mixed systems. In vivo, proteins never exist as isolated molecules, but they are immersed in crowded mixed environments where they fulfill their functions alongside other proteins and biomolecules (Alfano et al., 2024). A comparison of these concentrations across different organisms provides a 300–400 mg/mL range for E. coli and reports lower values for other organisms, with the lowest concentration being 9 mg/mL in rat kidney (Model et al., 2021). Thus, protein aggregation in the cell cytoplasm and in food products always occurs in crowded and heterogeneous conditions (Iwashita et al., 2017; Yan et al., 2008). The aggregation of food proteins, plays a crucial role in various food processing and cooking techniques, influencing texture, stability, and sensory characteristics (Mezzenga & Fischer, 2013; Zhu et al., 2022). Additionally, protein aggregation can impact the digestibility and nutritional quality of food, since aggregated proteins can alter digestive enzymes accessibility (Qin et al., 2024), influencing their bioavailability (Zhang et al., 2023). In particular, the possibility of employing amyloid fibrils as safe food ingredients has been recently evidenced (Xu et al., 2023). Understanding and controlling biomolecules interactions, whether they are small molecules (Zhao et al., 2024) or macromolecules, are crucial in food properties and processing techniques to achieve the desired quality. In food processes, protein aggregation can be easily

* Corresponding author.
** Corresponding author.
E-mail addresses: marco.paolantoni@unipg.it (M. Paolantoni), sara.catalini@unipg.it (S. Catalini).

https://doi.org/10.1016/j.foodhyd.2024.110863
Received 7 September 2024; Received in revised form 31 October 2024; Accepted 18 November 2024
Available online 21 November 2024

induced by thermal treatment that promotes protein unfolding and both specific (i.e. cross-β) and unspecific (i.e. hydrophobic) interactions. Gelation, resulting in the formation of a percolating protein network, occurs in the preparation of gelatins and certain dairy products. Whey proteins, such as β-lactoglobulin (BLG) and bovine serum albumin (BSA), are frequently utilized in food compositions for their capacity to create gels, emulsions, and foams, along with their high nutritional value (de Castro et al., 2017; Lazidis et al., 2016). Upon thermal treatment, mixtures of whey proteins can form irreversible gels, which are widely utilized in the food industry (Khalesi et al., 2021; Liu et al., 2024). Recently, composite gels are considered whose features can be effectively modulated by incorporating protein fibers within the hydrogel matrix (Khalesi et al., 2021; Liu et al., 2024). The properties of the composite gels ultimately depend on a complex interplay of intermolecular interactions, involving protein aggregates of various types and hierarchical organization at different spatial scales.

The heat-set aggregation of whey proteins has been the object of many investigations that concerned either the formation of amyloid fibrils in rather diluted conditions or the formation of particulate gels (Cao & Mezzenga, 2019; Jansens et al., 2019; Nicolai, 2019). Protein mixtures, involving BLG and BSA, have been also considered (Nicolai, 2019), showing that the partial substitution of BLG with BSA increases the denaturation rate of BLG and modulates the gelation features of the system (Ikeda & Morris, 2002; Kehoe et al., 2007). Nevertheless, the formation of amyloid aggregates in highly concentrated samples has been more rarely considered. Additionally, a molecular-level investigation concerning the formation of amyloid aggregates in crowded whey protein mixtures is still lacking, despite the relevant role these crowded protein mixtures may play in food and material sciences. A protein solution can be considered crowded when the average distance between the van der Waals surfaces of the monomers is like the size of a single protein (Laue, 2012). For instance, a serum albumin solution (pH = 7.5) at concentrations larger than ca. 70 mg/ml is expected to meet these conditions (Laue, 2012). The molecular crowding is expected to affect protein aggregation and amyloid formation, mainly in connection to excluded volume effects. Interestingly, it has been suggested that these latter might favor or disfavor fibril formation depending on the aggregation mechanism (Alfano et al., 2024).

Here, molecular and structural insights into the aggregation processes of BLG and BSA mixtures were obtained at low pH in diluted and crowded samples. In these conditions, both BLG and BSA tend to self-associate, forming amyloid and amorphous aggregates, respectively. Therefore, studying this mixture can also be useful for investigating potential changes in amyloid formation and gelation when different types of aggregation occur. In particular, aqueous solutions at pH 1.4 were examined at different BLG-BSA molar ratios, in a diluted regime (total protein content of 20 mg/ml) when BLG amyloid fibrils are produced after a prolonged thermal treatment. Moreover, analogous mixtures were investigated in highly concentrated samples (total protein content of 200 mg/ml). We have implemented various spectroscopic techniques, including Fourier transform infrared (FTIR), circular dichroism (CD), and deep Ultraviolet Resonance Raman (UVRR) to provide molecular scale information, while small-angle X-ray scattering (SAXS) was used to shed light on nanoscale structural details. The viscoelastic properties of the system, which ultimately depend on molecular interactions and the branching of nanoaggregates structuring, were examined using heterodyne transient grating (HD-TG) non-linear spectroscopy. We demonstrate that composite hydrogels, composed of amyloid aggregates of BLG and amorphous aggregates of BSA, can form within reduced time scales in the crowded regime. The presence of BSA does not affect the quantity of BLG amyloid aggregates but increases their formation rate. The mechanical strength of the gels formed from the different mixtures is related to the content of amyloid structures in the system.

2. Experimental section

2.1. Samples preparation

Lyophilized powders of β-lactoglobulin from bovine milk with a purity ≥90% (Sigma Aldrich, L0130-5G) and bovine serum albumin with a purity ≥96% (Sigma Aldrich, A2153-10G) are dissolved in deuterium oxide (99.9% D, Sigma Aldrich) to create solutions with varying protein concentrations and BLG-BSA molar ratios. Deuterated water is used for FTIR absorption measurements because the bending band of light water falls in the same spectral region as the amide signals, obscuring them. In contrast, in deuterated water these vibrational frequencies shift to lower values due to the increased molecular mass, thereby clearing the spectral region of interest. To enable consistent comparisons across all experimental data, we also used deuterated water in other experiments, including CD, UVRR, SAXS, and HD-TG. The diluted solutions are prepared by weighing the lyophilized protein powders to achieve a total protein concentration of 20 mg/mL, with variations in the molar ratio of BLG to BSA. Proteins are dissolved using a vortex mixer, and the pH of the solution is adjusted by adding deuterium chloride solution (2M) drop by drop to achieve a final pH of 2.0. Amyloid fibrils are generated from freshly diluted solutions placed in glass vials and maintained at 85 °C for 52 h under magnetic stirring, by adapting the protocol reported in literature (Heyn et al., 2019). For concentrated samples (total protein content of 200 mg/mL), a vortex mixer is utilized for protein solubilization, and the solution's pH is adjusted by adding deuterium chloride solution (2M) to achieve final pH values of 1.4. Amyloid hydrogels are prepared from freshly concentrated solutions and incubated at 85 °C for 2 h to obtain transparent gels.

2.2. FTIR

Infrared absorption measurements are conducted using a Bruker spectrometer model Alpha FTIR. The spectra are acquired through the Bruker Optics program Opus 7.5 and subsequently analyzed with Origin 2018 software. Samples are positioned in a custom-made cell equipped with calcium fluoride (CaF_2) windows, and the optical path length is adjusted using Teflon spacers. Once the sample is inserted between the windows, the cell is mounted inside a chamber controlled by a Peltier system. Spectra are collected with a resolution of 2 cm^{-1} by averaging 30 scans and are analyzed within the 1500–1700 cm^{-1} spectral range. To ensure consistency, the spectra are normalized by dividing each spectrum by the value of the amide I band area.

2.3. UVRR

UV Resonance Raman experiments were carried out at BL10.2-IUVS beamline of Elettra Sincrotrone Trieste (Rossi et al., 2020, 2022, pp. 183–225). The exciting wavelength at 226 nm was provided by the synchrotron radiation (SR) by adjusting the aperture of the undulator gap and employing a Czerny-Turner monochromator (Acton SP2750, focal length 750 mm, Princeton Instruments, USA) equipped with a holographic grating with 3600 grooves/mm to monochromatize the incoming SR. UVRR spectra are collected in a backscattered geometry using a single-pass Czerny-Turner spectrometer with a 750 mm focal length and a holographic grating with 1800 grooves/mm. The spectral resolution was set at about 1.6 cm^{-1}/pixel. Spectrometer calibration is standardized using cyclohexane (spectroscopic grade, Sigma Aldrich), which does not absorb UV within the wavelength range of interest. To mitigate possible photodamage effects or sample heating, the power radiation on the sample was kept at about 24 μW. Additionally, the sample cell is continuously horizontally shifted during measurements. Raman spectra of protein monomers, aggregates, and hydrogels are acquired at room temperature, while the kinetics of hydrogel formation are recorded at 85 °C. Temperature stability is maintained at a constant value with a precision of ±0.1 °C using a sample holder equipped with a

thermal bath attached to a resistive heating system. UVRR spectra of protein solutions are analyzed in the 1300–1700 cm^{-1} spectral region where the main signals of aromatic amino acids fall. For a better comparison the spectra have been arbitrarily normalized on the total intensity of the tyrosine band at ~1611 cm^{-1}.

2.4. CD

Circular dichroism spectra are recorded employing a Jasco J-810 polarimeter equipped with a plug-n-play single-cell Peltier with a stirrer for temperature control. Samples are placed in 0.1 mm quartz cuvettes. The spectra were recorded at room temperature. Each CD spectrum is an average of 10 scans recorded in the range from 185 to 270 nm, utilizing a scanning speed of 50 nm/min and a bandwidth of 2 nm. The measurements are carried out under a consistent nitrogen flow, utilized to purge the ozone generated by the instrument's light source. For each CD spectrum, the buffer alone (D_2O) was subtracted from the corresponding sample.

2.5. SAXS

SAXS analyses were conducted at the Austrian SAXS beamline in Elettra Synchrotron, Trieste (Italy). A 16 keV energy X-ray beam irradiated the samples, and the 2D Pilatus3 1M detector measured the scattered light in a q range from 0.09 to 8.1 nm^{-1}. Three different concentrations of protein samples were measured, each requiring a different sample holder. For higher protein concentrations (200 mg/mL solutions), special glass capillaries of 80 mm length and 1.5/1.6 mm diameter were used, loaded with a syringe. The measurements were performed at room temperature, followed by placing the capillaries in a thermal bath at a fixed temperature of 85 °C for 2 h to induce hydrogel matrix formation. After cooling, measurements on gels were acquired. To analyze other samples at diluted concentrations (20 mg/mL for solutions and fibrils) and highly diluted samples with a total concentration of 5 mg/mL to focus on a protein monomer, an autosampler was employed. This system features an automatic arm with a pipetting mechanism, moving over a PCR plate where pre-loaded samples are situated. The arm extracts 20 μL of solution, places it between two parallel windows, and conducts the analysis. An automatic cleaning system is then activated, allowing the loading of a new sample drop (Haider et al., 2021). The acquired data are processed using the average function and background subtraction (of D_2O solvent) through IgorPro software, and the SasView program is employed for data fitting.

2.6. SEM

Field emission scanning electron microscopy (FE SEM) using the LEO 1525 instrument by ZEISS is employed to investigate the morphology of the fibrils. A solution droplet is dispensed onto a silicon substrate using a glass Pasteur pipette and left to dry at room temperature for 12 h. Subsequently, the samples undergo metallization with an 8 nm chromium layer before being examined through SEM. The measurements are conducted with a 15 kV In-lens detector.

2.7. HD-TG

Heterodyne Transient Grating (HD-TG) is a time-resolved, non-linear spectroscopy technique that employs both pulsed and continuous-wave (cw) laser sources to investigate acoustic, structural, and thermal relaxation processes. The HD-TG experiments were conducted at the European Laboratory for Non-Linear Spectroscopy, University of Florence, and the complete scheme of the experiment has been described elsewhere (Cucini et al., 2010a, 2010b; Taschin et al., 2006). In TG experiments, the output of a 20 ps pulse, 10 Hz repetition rate Nd YAG laser operating in the fundamental (1064 nm) is divided by a phase mask into two pulses that interfere, generating an impulsive spatial modulation of the material's optical properties, defined by the wave vector q. A third beam (probe) of a 532 nm cw laser, is utilized to monitor the time evolution of the induced modulation. By varying the spacing of the grooves on the phase mask, different angles between the exciting beams are produced, altering the q-vector in the sample. The effects of q-vector values of 2.1 μm^{-1} is examined. A third cw laser beam with a wavelength of 532 nm probes the time evolution of the transient induced grating. The sample grating diffracts the probe beam, and the resulting diffracted beam constitutes the experimental signal. The optical setup includes a pair of achromatic doublets and a phase control device that facilitates heterodyne detection through the beating of the signal with a reference beam. A photodiode with a bandwidth of 1 GHz measures the HD-TG signal after optical filtering. The signal is amplified and recorded using a digital oscilloscope with a bandwidth of 7 GHz. Each signal is an average of 1000 records, ensuring a high signal-to-noise ratio. The samples are retained directly in the cuvette, placed in a copper cell holder, and coupled to a thermostat and a thermocouple for temperature feedback. The parameters discussed in the manuscript include the speed of sound (C_s) and the damping rate (Γ_A), both extracted from the oscillating part of the HD-TG signal (Catalini et al., 2019). The speed of sound is calculated as $C_s = \omega_A/q$, and the damping rate is calculated as $\Gamma_A = 1/\tau_A$. The parameters ω_A and τ_A are the angular frequency and the damping time of the acoustic wave oscillation and q is the scattering vector imposed by the experimental geometry. The uncertainty associated with C_s is 0,1% and that associated with Γ_A is 1%, both are related to the fitting procedure.

3. Results and disussion

3.1. Amyloid fibrils in diluted regime

3.1.1. Molecular interactions and conformation

In the low concentration regime (total protein amount 20 mg/mL), a molecular characterization of the protein solutions was conducted using three distinct spectroscopic techniques: FTIR, CD and UVRR. The results obtained are reported in Fig. 1. For each protein solution, we compare the spectra collected at room temperature, both before and after the thermal treatment used to produce the amyloid fibrils, as described in paragraph 2.1.

The FTIR spectra of the analyzed protein mixtures are depicted in Fig. 1a–e in the spectral range where the distinctive amide I (AI) and amide II (AII) bands fall. The AI band, attributed to carbonyl stretching vibration, appears around 1650 cm^{-1}. The spectral variations of this signal can be correlated with the modifications of the secondary structure of the proteins. All the spectra are arbitrarily normalized to the AI band area. The AII band, associated with CNH bending vibration, is observed at approximately 1550 cm^{-1} for the BLG sample. When the proteins are dissolved in deuterium oxide (D_2O), the deuterium atoms (D) replace the amide hydrogen atoms (H) through an exchange process, thereby altering the AII band frequency. However, when BLG maintains its globular state, only the exposed H atoms undergo exchange, resulting in a residual AII band intensity (black curve in Fig. 1a). Following thermal treatment, the AII band disappears (red curve in Fig. 1a), because BLG has undergone a folding transition. Furthermore, this thermal treatment causes the appearance of a new band at 1618 cm^{-1}, indicating the formation of specific intermolecular cross-β interactions characteristic of amyloid-type aggregate structures (Catalini et al., 2021, 2022, pp. 183–225; Dobson, 2004; Foley et al., 2013; Venturi et al., 2023).

Concerning UVRR, we employed a 226 nm excitation wavelength, leading to a selective enhancement of signals associated with aromatic amino acids, i.e. Tyrosine (Tyr), Tryptophan (Trp), and Phenylalanine (Phe) (Ahmed et al., 2005; Asher et al., 1986; Chi & Asher, 1998a). In the present case, two specific bands related to Trp and Tyr are considered (Ahmed et al., 2005; Asher et al., 1986; Chi & Asher, 1998a, 1998b; López-Peña et al., 2015). The first, situated at about 1611 cm^{-1},

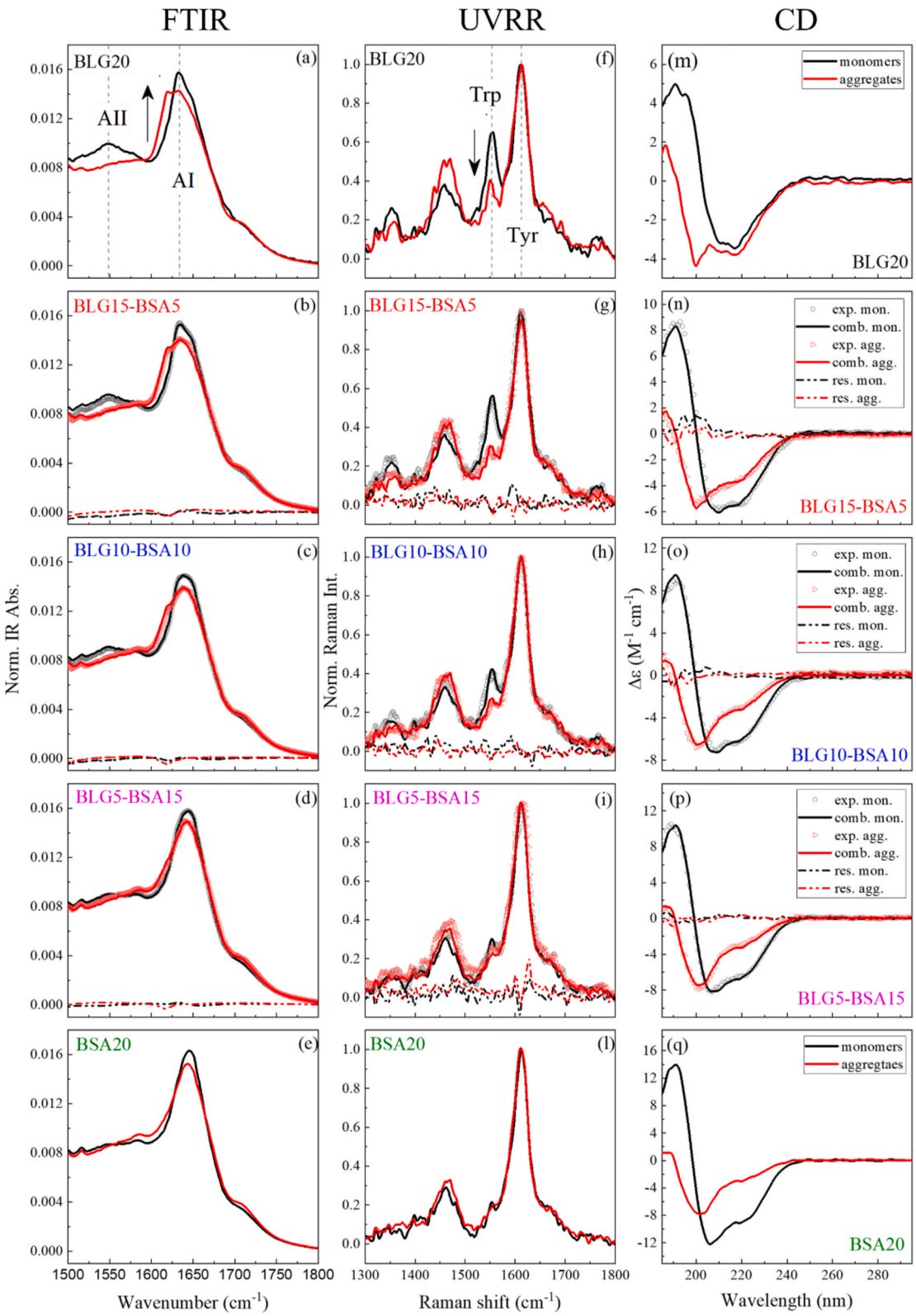

Fig. 1. FTIR absorption spectra normalized to the area of amide I band (a–e), UVRR scattering spectra normalized to the intensity of the tyrosine band (f–l) and CD absorption spectra(m-q) of monomers and aggregates of the pure BLG and BSA solutions and their mixtures at different molar ratio keeping fixed the total protein concentration at 20 mg/mL. Spectra of monomers (black line) and aggregates (red lines) are recorded at room temperature. The experimental spectra of the mixtures are plotted as open black circles (labeled 'exp. mon.' for the experimental spectra of monomers) and open red triangles (labeled 'exp. agg.' for the experimental spectra of aggregates). The curves from the linear combination of the pure proteins are overlaid on the experimental data, labeled 'comb. mon.' and 'comb. agg.' representing the combined spectra of pure BLG and BSA monomers and pure BLG and BSA aggregates, respectively. The residuals, shown as dashed lines, were calculated as the difference between the experimental curve and the fit and are labeled 'res. mon.' and 'res. agg.' to indicate the residuals for monomers and aggregates, respectively.

corresponds to the in-plane stretching vibration mode of the Tyr ring. The second, at 1556 cm^{-1}, originates from the stretching mode between C2-C3 of the pyrrole ring of Trp (Venturi et al., 2023). Fig. 1f shows that after the thermal treatment the relative intensity of the Trp band strongly decreases with respect to Tyr signal. This change can be related to variations of the chemical environment around the selected groups during the aggregation process (Kurouski et al., 2010, 2012, 2015; López-Peña et al., 2015; Shashilov et al., 2007; Xu et al., 2008). Specifically, the decrease in the intensity of the Trp signals can be linked to the formation of hydrogen bonds by the indole ring, which causes a blue shift in the electronic band. This shift reduces the resonance effect, leading to a corresponding decrease in the intensity of the Trp Raman signals (Schlamadinger et al., 2009). For BLG it represents a specific marker of the modulation on the Trp environment due to amyloid aggregates formation (Venturi et al., 2023).

The CD spectrum collected before the thermal treatment (monomeric species) is shown in Fig. 1m. It reveals characteristic features related to different types of secondary structure in the Far UV region (Kelly et al., 2005). In particular, the CD spectrum of the BLG solution exhibits a negative minimum at 218 nm, indicative of a β-sheet conformation, consistent with its known native structure (Dave et al., 2013). After thermal treatment, the CD spectra minimum shows reduced ellipticity and shifts to around 200 nm. A similar blue shift and decrease in ellipticity were observed in thermally treated BLG and whey protein solutions, linked to the loss of α-helices and β-sheets and an increase in disordered structures (Herneke et al., 2021; Lara et al., 2011; Tomczyńska-Mleko et al., 2014). This finding is further supported by reproducing the CD spectra for both the solution and fibrils using the BestSel program (fitting reported in Fig. S1 of the supporting information, SI). For secondary structure analysis, BestSel fits the CD spectrum of an unknown protein with a linear combination of eight pre-calculated basis spectra, each representing a distinct secondary structure component. The results, with an associated error of about 2%, indicate a trend of more ordered structures converting into more disordered structures. The percentages of the secondary motifs (Qin et al., 2023) have been summarized in table T1.

The BSA at pH 2.0 is expected to adopt an extended conformation (E-form) that is mostly unfolded, allowing for a fast H/D exchange (Comez et al., 2021). In fact, the AII band in the FTIR spectrum of pure BSA (Fig. 1e) is not present, confirming its unfolded state. In this case, only minor spectral changes are observed after the thermal treatment, and the formation of amyloid species is negligible. The UVRR spectrum of the starting solution (Fig. 1l) does not present the Trp band, and no variations are observed after the thermal treatment. The CD spectrum (Fig. 1q) collected before the thermal treatment (BSA monomers) shows two negative minima at 208 nm and 222 nm compatible with the BSA extended conformation (Varga et al., 2016). Notably, significant spectral changes are observed after thermal treatment, indicating irreversible conformational changes likely due to the formation of non-specific (amorphous) aggregates. The minimum at 200 nm may correspond to unordered fragments, as the BestSel results (Fig. S1 and Tab. T1) show a conversion of many helical motifs into disordered structures and β-motifs. Interestingly, the spectra of the BLG-BSA mixtures (empty symbols in Fig. 1), measured with the three techniques, can be well reproduced by the weighted sum of the spectra of the pure systems (full lines spectra in Fig. 1), where the weight factors scale with the relative proteins quantity. This good overlap of the experimental curves with the calculated ones is achieved for the solutions both before and after the thermal treatment. From this observation we can deduce that the two proteins do not tend to form mixed fibrillar aggregates. Moreover, at a molecular level, the presence of a given protein in the mixture does not alter significantly the conformational and aggregation properties of the other.

3.1.2. Structural characterization

To monitor the three-dimensional structures resulting from the aggregation of BLG and BSA, we conducted synchrotron SAXS measurements at the onset and at equilibrated aggregation processes, for different BLG-BSA samples in D_2O (pH = 2.0) at 20 mg/mL total protein content. SAXS is a well-assessed method for the structural characterization of both ordered and disordered proteins in solution.

Fig. 2a and e depict the SAXS spectra of pure BLG and BSA solutions, respectively, used as reference curves. The scattering intensity I(q) of dilute protein solutions (5 mg/mL) is reported in Fig. S2. The related curve-fitting analysis, performed using a spherical model (explained in the SI), yields for the diluted BLG solution a radius of ~2.0 nm that is consistent with the average size expected for BLG dimers (Anghel et al., 2019). In fact, the BLG oligomerization is highly dependent on pH and ionic strength, and dimers form at pH values ranging from 2.0 to 4.5 (Anghel et al., 2019). The SAXS curve of the 20 mg/ml BLG solution can be instead reproduced considering the combination of a spherical from factor and a RMSA potential (Fig. 2a), as technically explained in the SI. A bump can be clearly observed at q = 0.32 $Å^{-1}$ (d = 19.6 Å), it represents a characteristic length of the BLG globule.

The I(q) profile for the BSA solution (20 mg/mL) at pH 2.0 is reported in Fig. 2e. This is reproduced considering a flexible cylinder model implemented in SasView program (Fig. S1e), leading to a contour length of approximately 20.0 nm. Notably, the known maximum size of BSA in its native conformation is approximately 10.0 nm (Barbosa et al., 2010). Thus, the findings confirm that BSA is present in the extended conformation, characterized by an increased hydrodynamic radius, due to molecule elongation (Babcock & Brancaleon, 2013), and that the extended conformation does not spontaneously assemble into large-scale ordered aggregates, such as fibrils. The bump at q = 0.32 $Å^{-1}$ observed for BLG is not present in this case.

The SAXS curves of protein mixtures (Fig. 2b–d) collected before the thermal treatment, can be suitably reproduced by a combination of the pure protein solutions profiles, adjusted by a factor accounting for the relative protein content, in agreement with FTIR, UVRR and CD outputs.

Kratky plots of SAXS intensity data are commonly used for qualitative assessment of protein chain flexibility. These plots (Fig. 2f–l) show that the BLG is folded into a compact globule while BSA is less compact, making the corresponding distribution profile less bell-shaped and structured. The data also suggest that both proteins maintain the same structuring in the mixtures.

The SAXS curves obtained after incubation at 85 °C for 52 h (Fig. 2a–e red curves) exhibit an increase of I(q) at low q values and a corresponding slope change, suggesting the formation of aggregates. For the BLG20 sample, the slope is −1.6, the same value has already found for insulin amyloid fibrils (Siposova et al., 2022), confirming that BLG aggregates are of fibrillar nature. Increasing the BSA concentration causes a reduction of the slope, reaching the −0.2 value for the pure BSA solution. In this case the formation of amorphous BSA aggregates can be envisaged. Regarding the Kratkly plots (Fig. 2f–l), the differences between the curves obtained before and after the thermal treatment are more pronounced when the sample contains a larger fraction of BLG, which is expected to assemble in fibrillar structures.

3.1.3. Aggregates morphology

To shed light on the morphology of the aggregates after the thermal treatment, SEM images of the protein samples are acquired and reported in Fig. 3.

Pure BLG (Fig. 3a and f) forms numerous tiny fibrils, consistently with the findings of previous studies in which similar protocols were employed (Hoppenreijs et al., 2022; Lara et al., 2011).

Fig. 3e and l refer to pure BSA and reveal the formation of unordered aggregates with a lamellar-like morphology. Mixed samples containing both BLG and BSA exhibit the presence of fibrillar species with slight variations in diameter, depending on the BLG-BSA molar ratio. BLG15-BSA5 and BLG10-BSA10 samples (Fig. 3g and h, respectively), display fibers with a larger diameter and a wrinkled, jagged surface. This observation, coupled with spectroscopic results, suggests that the fiber skeleton primarily forms through the cross-β association of BLG.

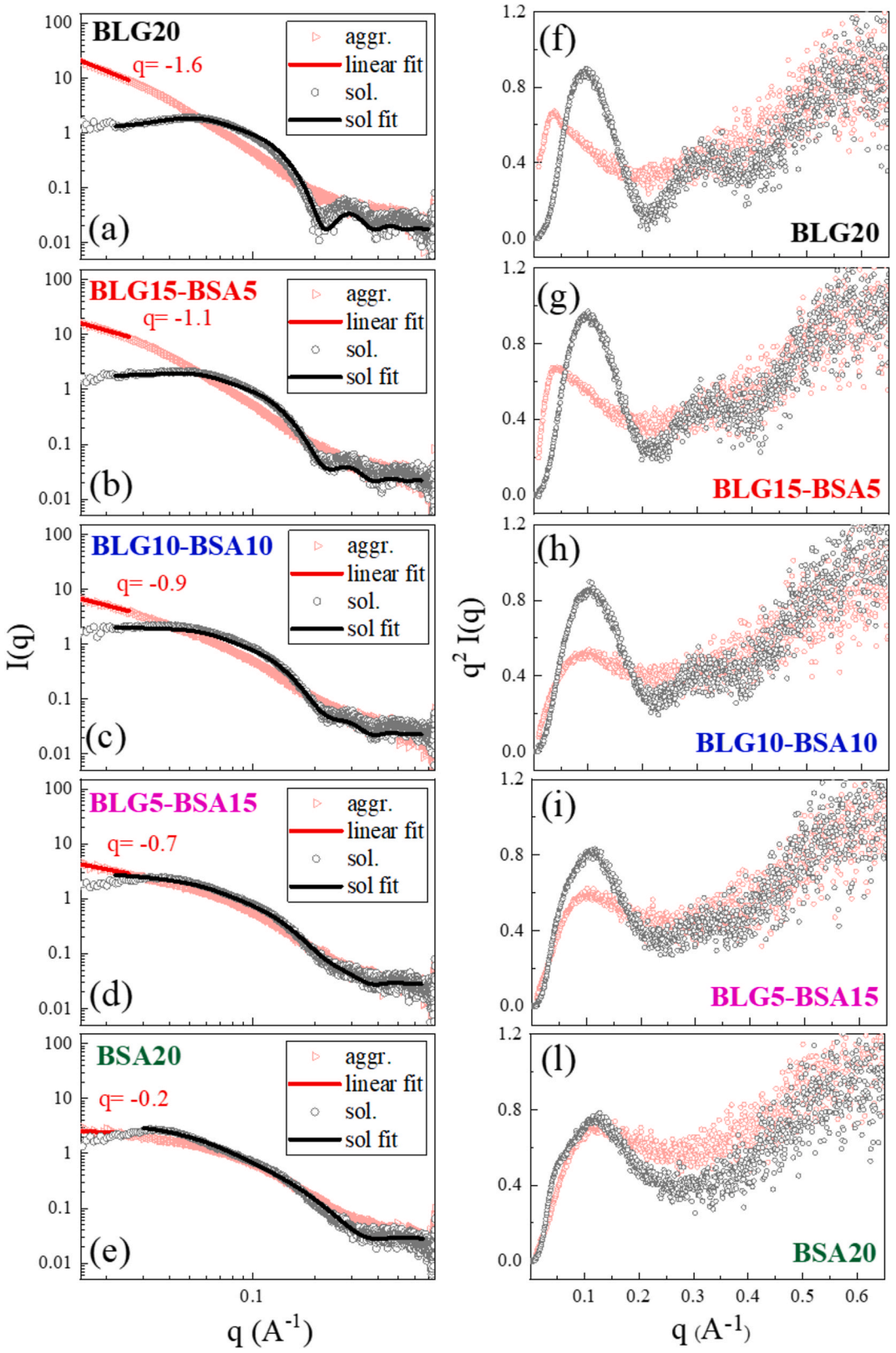

Fig. 2. Here, we present the X-ray scattering intensities: black circles represent monomers (labeled 'sol.' for experimental curves of the monomer solution), and open red triangles represent aggregates (labeled 'aggr.' for experimental curves of the aggregates). The SAXS curves for individual BLG and BSA proteins, as well as their mixtures at varying molar ratios, are shown with a total protein concentration of 20 mg/mL. The left panels (a–e) display the I(q) data on a log-log scale, while the right panels (f–l) show the Kratky plots, represented as $q^2I(q)$. The experimental data are fitted with curves, which are reported as solid-colored lines.

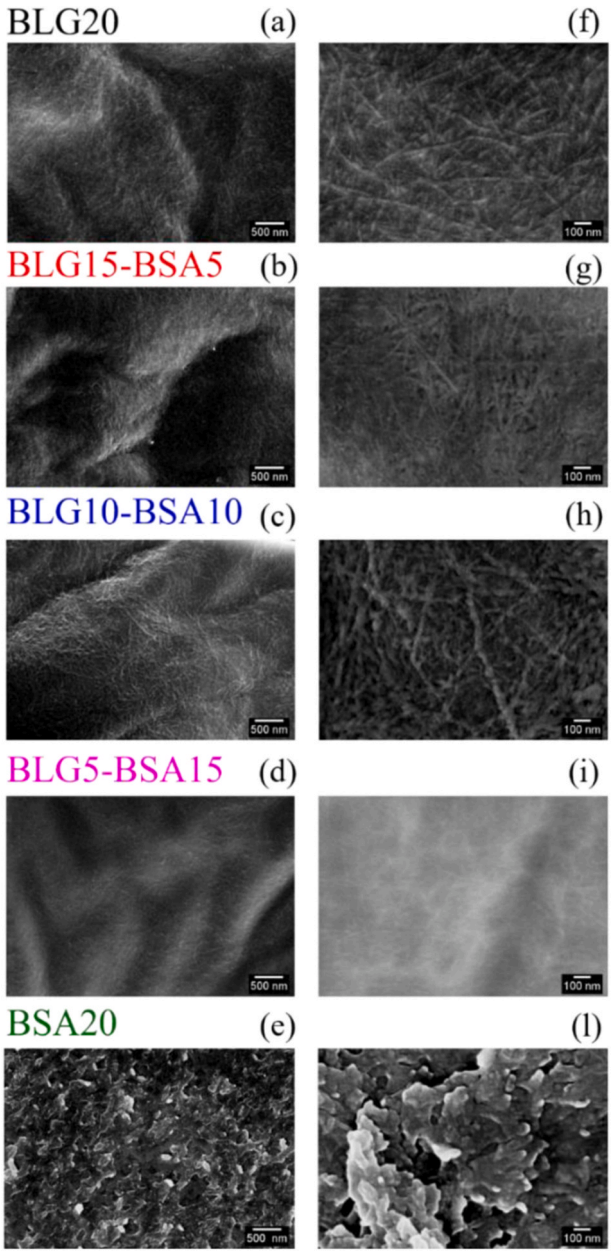

Fig. 3. SEM images at 50 k (a–e) and 150 k (f–l) magnification of the dried aggregates of the single BLG and BSA and their mixtures at different molar ratio keeping fixed the total protein concentration at 20 mg/mL. The 500 nm and 100 nm length are reported on (a–e) and (f–l) panels, respectively.

However, BSA tends to wrap around this skeleton, thickening the fibers diameter. Thus, BLG chains engage in cross-β interactions with other BLG chains, resulting in ordered amyloid fibrils, while BSA molecules preferentially interact with other BSA molecules, leading to the formation of amorphous aggregates. These amorphous aggregates, likely driven by a strong hydrophobic effect, tend to wrap around the fiber skeleton, through non-specific interactions, yielding fibers with a thicker morphology and an irregular surface.

3.2. Hydrogel networks in crowded regime

3.2.1. Hydrogel formation kinetics and molecular interactions

We now turn our attention to the high concentration regime, which is characterized by a total protein concentration of 200 mg/mL. For this sample, the thermal treatment of protein solutions consists in keeping the samples at 85 °C for 2 h. In this densely populated condition, the rate of amyloid formation increases, leading to the formation of a hydrogel matrix. The progress of the formation of intermolecular β-sheet is tracked collecting FTIR spectra as a function of the incubation time. A fitting procedure (Fig. S4) utilizing three Voight bands is employed to estimate the relative intensity of the signals in the spectral range between 1600 and 1700 cm^{-1} (AI band) that relates to the fraction of groups involved in cross-β structures. The results of this analysis are shown in Fig. 4, with details on the function and technical explanation of the fitting procedure provided in the Supporting Information (Fig. S4).

The final cross-β percentages scale proportionally with the BLG concentration, mirroring the behavior observed for fibrils in the low concentration regime. By looking at the trends reported in Fig. 4a, all the samples, except BLG100, reach a plateau after 120 min. The comparison between the blue and gray curve, representing the BLG100-BSA100 and BLG100 samples, respectively, indicates that the presence of BSA influences the amyloid aggregation rate, while the final aggregate percentage is basically the same. In fact, BLG150-BSA50 shows the maximum aggregation rate. Overall, the data confirm that BSA does not directly contribute to the formation of amyloid species but affects the kinetics of their formation.

Similarly to the case of diluted solutions, the FTIR and UVRR spectra of concentrated samples have been collected at room temperature (Fig. 5) to provide molecular information about the concentrated protein solutions and hydrogels.

Also in this case, the FTIR and UVRR spectra of the solutions and the gels of the mixtures can be well reproduced considering the combination of the spectra of the single protein systems. This indicates the absence of any relevant mutual influence in determining the conformational and aggregation features after the thermal treatment, even in very concentrated samples.

FTIR data (Fig. 5a–e) indicate that going from the solution to the gel leads to the appearance of the cross-β signal (at 1618 cm^{-1}). This is only present in the spectrum of the gels (Fig. 5a–e), being more prominent in samples with increased BLG concentrations. At the same time, the UVRR spectra (Fig. 5f–l) point out that the intensity of the Trp band at ~1556 cm^{-1}, mainly attributed to BLG, decreases when moving from the solution to the gel. Fig. 5m displays in the same graph the estimated percentage of cross-β linkages (black points) and the percentage intensity of the Trp signal (red points) reduction ($[I(Trp)_{sol}-I(Trp)_{gel}]/I(Trp)_{sol}$) as a function of the BLG-BSA molar ratio. It is noteworthy that the trend exhibited by these two quantities is qualitatively the same. This further confirms that the Trp residue in BLG is involved in the formation of amyloid interactions (Kurouski, Van Duyne, & Lednev, 2015).

3.2.2. Hydrogels structure

To explore how the protein aggregation affects the resulting hydrogel network, we carried out SAXS measurements on the concentrated protein solutions and hydrogels (see Fig. 6). SAXS curves of proteins solutions at 5 mg/mL, 20 mg/mL and 200 mg/mL are plotted together and reported in Fig. S3.

A qualitative assessment of the scattering curves suggests that there are significant structural differences between pure BLG and BSA hydrogels and hydrogels formed starting by mixed solutions (Hughes et al., 2021). The relative increase of BSA content results in a reduction of scattering intensity at low q values and in a change of curve slope, which is different form that observed when aggregates were formed at lower concentrations (Fig. 2). Moreover, as before, with increasing the BSA content the difference between solution and gel curves becomes less marked, as also evidenced by corresponding Kratky plots. The SAXS curve of the gels are well reproduced in the low q region up to ca. 0.2 $Å^{-1}$ through an empirical functional form (the correlation length model), implemented in the SasView program. The used fitting function reasonably reproduces the experimental data, providing characteristic correlation lengths ranging from 24.5 ± 0.1 Å to 17.0 ± 0.1 Å, passing from the pure BLG matrix to the pure BSA matrix, respectively. The

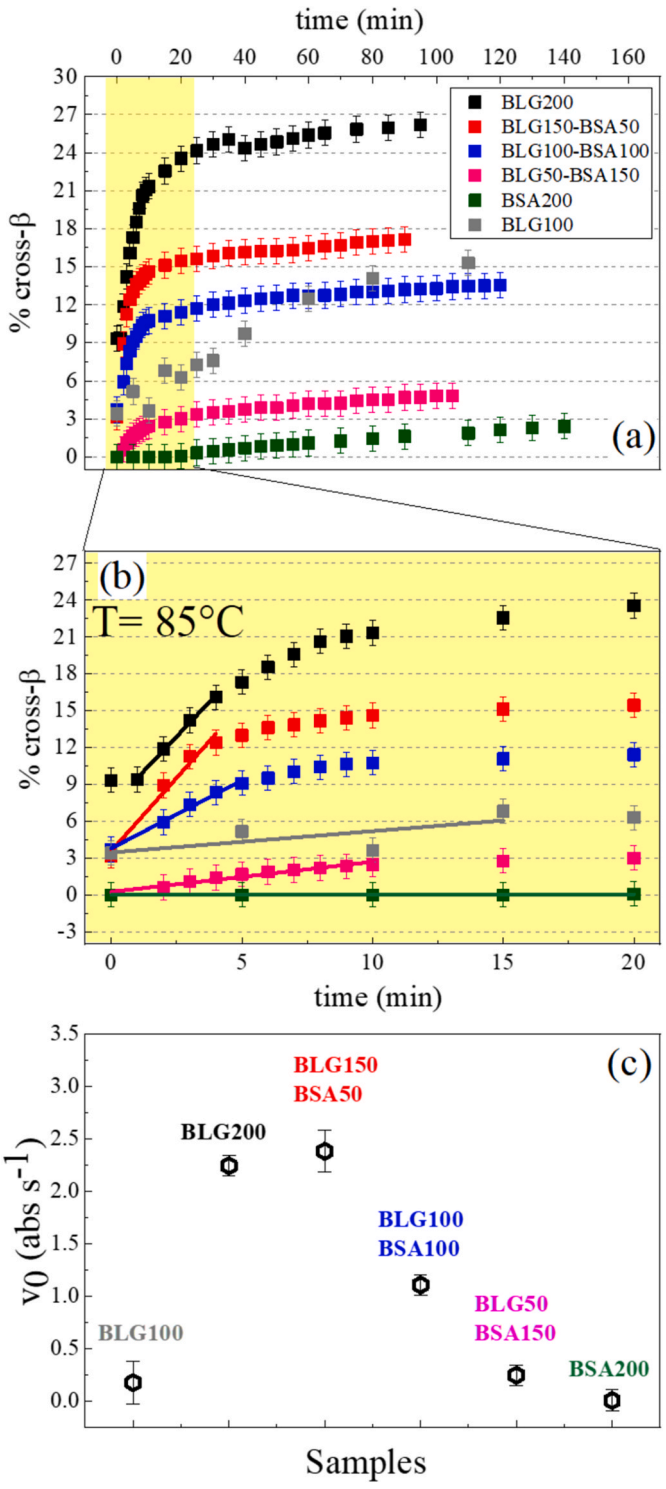

Fig. 4. percentage of cross-β estimated through a fitting procedure of the FTIR spectra. During the thermal treatment at 85 °C of the pure BLG and BSA and their mixtures at different molar ratio (total protein concentration fixed at 200 mg/mL).

simple model employed provides qualitative insights on the structural changes of hydrogels. As a result, we can argue that the gel matrix created by BLG has a higher characteristic correlation length because it is formed by an ordered fibrillar network (Anghel et al., 2019; Moitzi et al., 2011). On the other hand, the one formed by BSA involves disordered non-fibrillar aggregates, leading to shorter characteristic correlation lengths.

3.2.3. *Hydrogels viscoelastic properties*

Finally, the viscoelastic properties of our systems have been analyzed by using time-resolved TG spectroscopy. The sound velocity, *Cs*, and the damping rate, Γ_A, are extrapolated from the TG oscillating signal (Catalini et al., 2019), and reported in Fig. 7.

Concerning the sound velocity, which describes the propagation of the acoustic wave into the materials, we obtain an average value of $Cs \simeq 1469$ km/s $\pm$ 0.001 for the concentrated solutions and Controlla $Cs \simeq 1475$ km/s $\pm$ 0.001 for the gels (Fig. 7a). The data indicate that the speed of sound in all the protein solutions is practically the same, independently on the molecular weight and volume of BLG and BSA (Amirkhani et al., 2011). An overall increase of *Cs* occurs for the hydrogels with respect to the protein solutions (Fig. 7a). This reflects an increment of the elasticity of the system which appears to be more solid-like. However, among the different gels, the value of *Cs* remains similar within the experimental errors, suggesting similar density and elastic properties of the different hydrogels. On the other hand, Γ_A results much more sensitive to the type of gel matrix (Fig. 7b). We note that for the concentrated solutions, the slight increase of Γ_A going from pure BLG to pure BSA, can be associated to an increase of the viscosity. In fact, the higher viscosity of the pure BSA sample can be related to the propensity of the extended conformation to create non-amyloid aggregates. Interestingly, the most significant variation of Γ_A occurs upon the formation of fibrillar gels. As a matter of fact, the Γ_A increment going from the solution to the hydrogels nicely correlates with the content of amyloid fibrils within the matrix. In other words, the acoustic wave is much more efficiently dampened when the gel contains a larger fraction of fibrils which, in turn, is higher on increasing the BLG fraction in the mixture.

4. Conclusion

Heat-set hydrogels composed of whey protein mixtures have recently garnered attention as promising systems in food technology and biotechnology (Khalesi et al., 2021). The addition of protein nanofibers for the reinforcement of whey protein gels has also been proposed (Liu et al., 2024). The properties of these composite gels depend on a complex hierarchy in their formation process involving the denaturation and aggregation of different proteins, ultimately shaping the multi-scale organization of the gel matrix and its mechanics. By adjusting the amyloid content in the composite gels, we can fine-tune the structural and viscoelastic properties of the system. Exploring the potential applications of these gels in the food industry could be highly promising, since BLG and BSA are able to provide essential amino acids for complete nutrition and high digestibility. However, it is important to consider that protein digestion kinetics and overall digestibility can be influenced by factors such as the protein native structure and aggregation, which may limit enzymatic access and impact protein solubility (Jaeger et al., 2024).

In the present study, composite gels of partial fibrillar nature were easily obtained in crowded BLG-BSA mixtures by eating treatment at low pH. Molecular, structural and mechanical information on the thermally-induced aggregation and gelation were derived under both diluted and concentrated conditions, using several spectroscopic approaches. We demonstrate that BLG exists in a globular state and associates upon thermal denaturation, forming amyloid fibrils with a long and thin structure. Tryptophan residues are found to contribute to the stabilization of the fibrillar cross-β architecture. In contrast, BSA adopts an extended form exposing all hydrophobic moieties to the solvent. Upon thermal treatment it fails to originate intermolecular β-sheets, forming instead unordered species with a lamellar-like morphology. Interestingly, the presence of a given protein in the mixed systems does not change the conformational and aggregation properties of the other at short (molecular) scales. On the other hands, fibrils formed in heterogeneous conditions are thicker and exhibit an irregular surface compared to those formed by pure BLG. BSA amorphous aggregates,

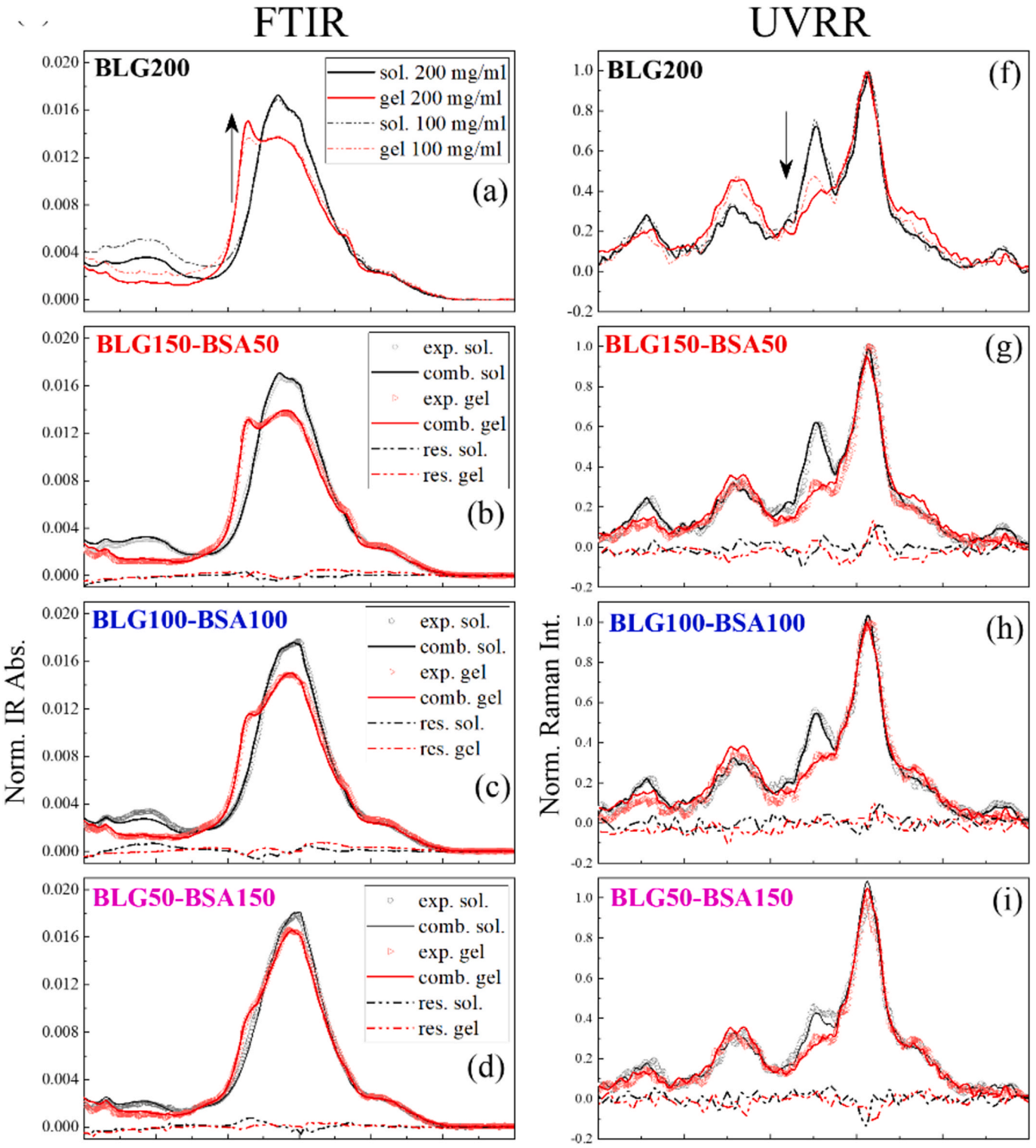

Fig. 5. FTIR absorption spectra normalized for the area of amide I band (a–e), UVRR scattering spectra normalized for the intensity of the tyrosine band (f–l) and percentage of cross-β and Trp intensity reduction (m) of hydrogels of the single BLG and BSA and their mixtures at different molar ratio keeping fixed the total protein concentration at 200 mg/mL. The experimental spectra of the mixtures are plotted as open black circles (labeled 'exp. sol.' for the experimental spectra of solution) and open red triangles (labeled 'exp. gel' for the experimental spectra of gels). The curves from the linear combination of the pure proteins are overlaid on the experimental data, labeled 'comb. mon.' and 'comb. agg.' representing the combined spectra of pure BLG and BSA monomers and pure BLG and BSA aggregates, respectively. The residuals, shown as dashed lines, were calculated as the difference between the experimental curve and the fit and are labeled 'res. mon.' and 'res. agg.' to indicate the residuals for monomers and aggregates, respectively.

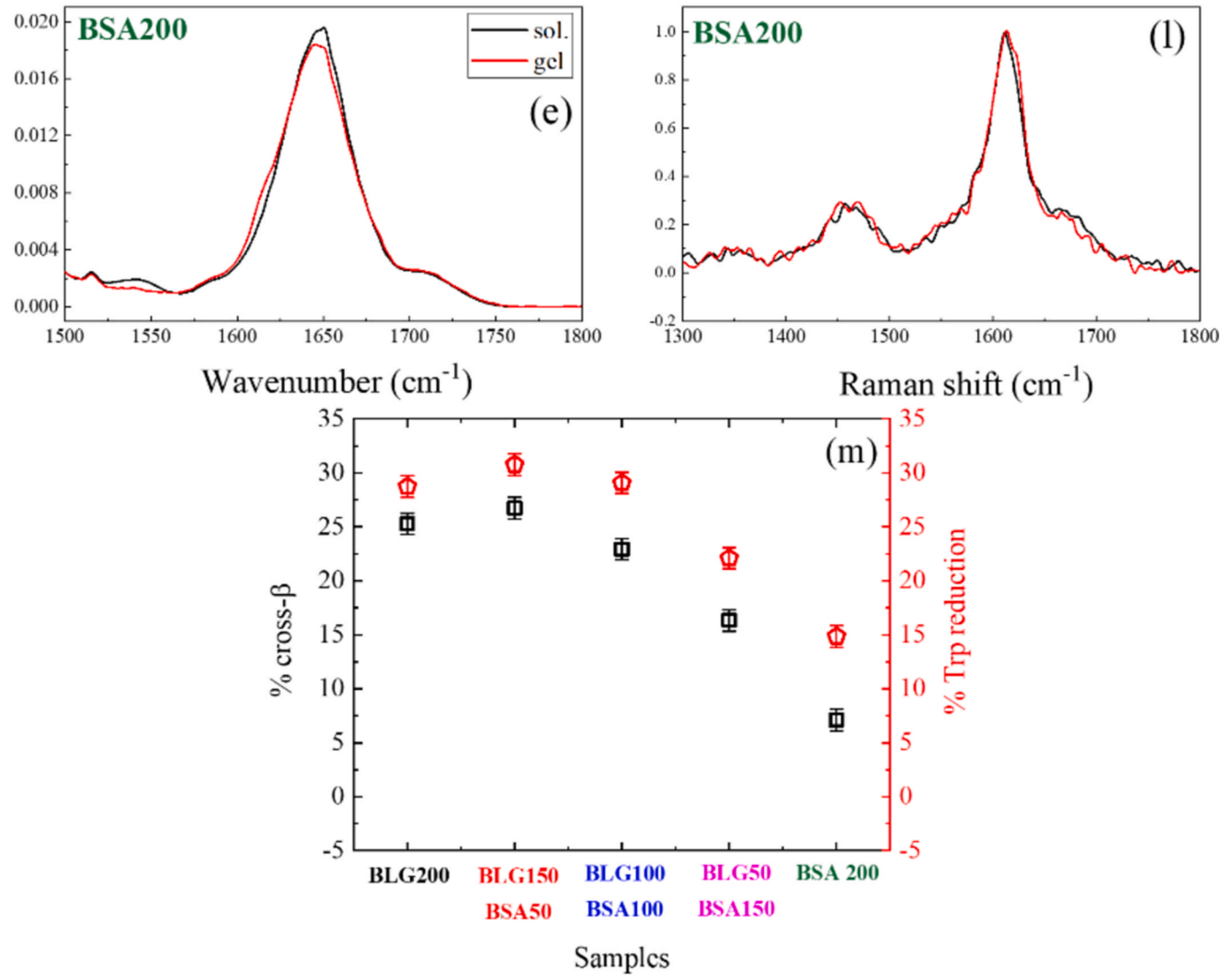

Fig. 5. (*continued*).

likely induced by a strong hydrophobic effect, seem to envelop the fiber skeleton, altering its morphology.

As the protein concentration increases, the aggregation process triggered by thermal treatment accelerates, reaching a stationary state after 120 min. The system percolates upon subsequent cooling, leading to the formation of different composite hydrogels. Substitution of BLG with BSA in the mixtures expedites the formation of BLG amyloid aggregates without affecting their final amount. Moreover, in the hydrogels containing a higher BSA content, the characteristic correlation lengths are shorter, and the viscosity is lower. Our findings indicate that the higher mechanical strength of the gels appears to stem from the BLG fibrillar network. BLG and BSA preferentially interact with themselves, forming amyloid- and non-amyloid-based hydrogels, respectively. However, the presence of BSA accelerates the BLG amyloid aggregation process, which in turn alters the nanometric structure of the final hydrogel matrix and its mechanical strength.

Notably, controlling the viscosity in hydrogels intended for food products is essential, as it significantly influences texture, stability, and mouthfeel, critical factors for consumer acceptance (McClements, 2024). Higher viscosity helps maintain a product's structural integrity, preventing phase separation and ensuring uniform consistency. Additionally, optimal viscosity can enhance processing and packaging efficiency, making the product more appealing and convenient for both manufacturers and consumers.

CRediT authorship contribution statement

Sara Venturi: Writing – review & editing, Writing – original draft, Visualization, Validation, Investigation, Formal analysis, Data curation, Conceptualization. **Barbara Rossi:** Writing – review & editing, Visualization, Validation, Resources, Investigation, Formal analysis, Data curation, Conceptualization. **Fatima Matroodi:** Writing – review & editing, Validation, Investigation, Formal analysis, Data curation. **Renato Torre:** Writing – review & editing, Resources. **Andrea Lapini:** Writing – review & editing, Resources. **Paolo Foggi:** Writing – review & editing, Resources. **Alessandro Di Michele:** Writing – review & editing, Resources. **Paola Sassi:** Writing – review & editing, Visualization, Formal analysis, Data curation. **Marco Paolantoni:** Writing – review & editing, Writing – original draft, Visualization, Validation, Supervision, Formal analysis, Data curation, Conceptualization. **Sara Catalini:** Writing – review & editing, Writing – original draft, Visualization, Validation, Supervision, Resources, Project administration, Investigation, Funding acquisition, Formal analysis, Data curation, Conceptualization.

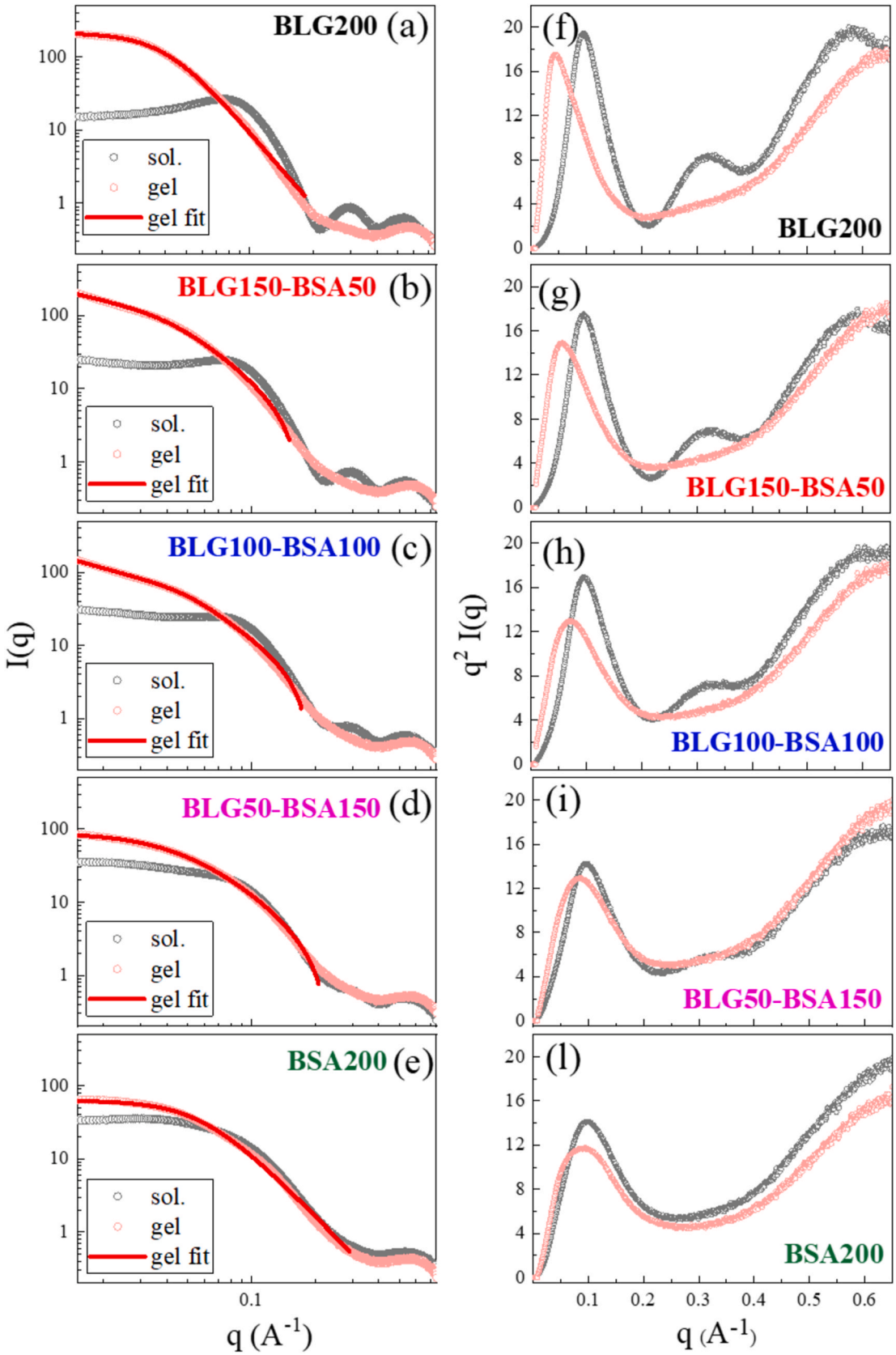

Fig. 6. Here we report the x-ray scattering intensities for solutions open black circles (labeled 'sol.') and for hydrogels open red triangles (labeled 'gel') of the single BLG and BSA proteins, as well as their mixtures at different molar ratio, with the total protein concentration maintained at 200 mg/mL. The left panels (a–e) display the I(q) data on a log-log scale, while the right panels (f–l) show the Kratky plots, represented as $q^2I(q)$. The experimental data of the hydrogels are fitted with empirical curves implemented in SasView, which are reported as solid-colored lines (labeled 'gel fit').

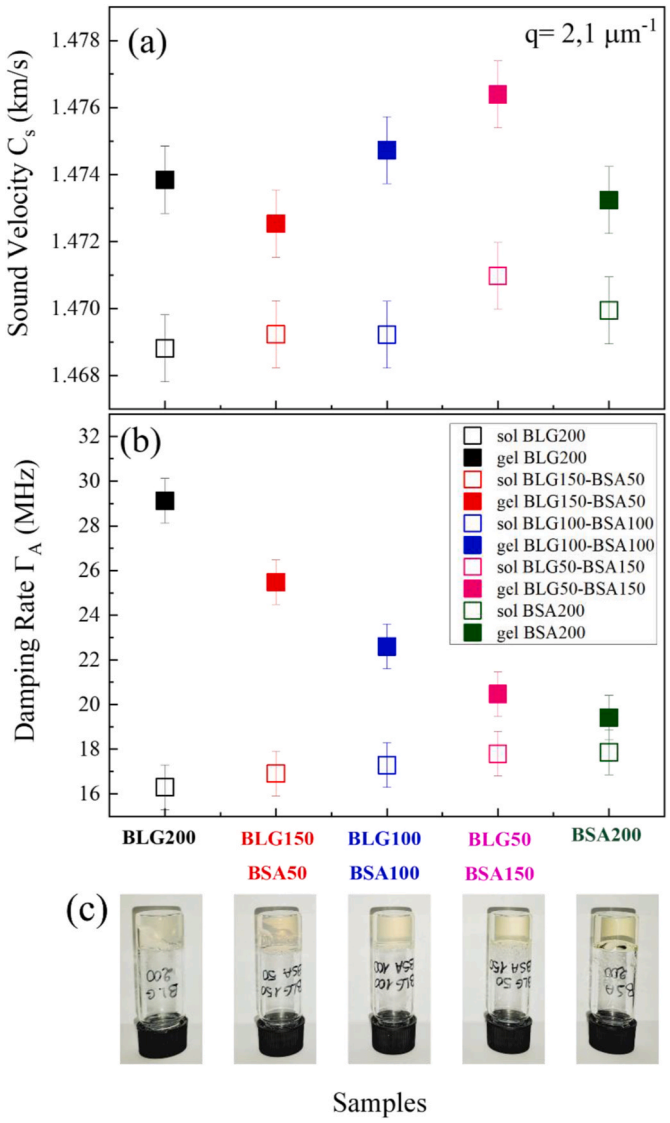

Fig. 7. Sound velocities (a) and acoustic damping rate (b) measured by HD-TG at the 2.1 μm^{-1} q-vector of solutions and hydrogels of the single BLG and BSA proteins and their mixtures at different molar ratio keeping fixed the total protein concentration at 200 mg/mL. Photos of the final gels are shown in panel (c). The gels formed are transparent but as the BSA content increases, a yellowish color of the matrix becomes evident.

Declaration of competing interest

The authors declare that they have no known competing financial interests or personal relationships that could have appeared to influence the work reported in this paper.

Acknowledgments

We acknowledge Elettra Sincrotrone Trieste for providing access to its synchrotron radiation facilities and for financial support under the SUI internal project (proposal number 20220424). The authors acknowledge the CERIC-ERIC Consortium for the access to experimental facilities and financial support (proposal number 20227195). The authors are grateful to Heinz for the assistance on SAXS beamline. S.C. thank the research project "FSE-REACT EU '' financed by National Social Fund–National Operative Research Program and Innovation 2014–2020 (D.M. 1062/2021), personal Grant number 23-G-15445-3. P.F., A.D.M., P.S., M.P., and S.C. thank the European Union-NextGenerationEU project under the Italian Ministry of University and Research (MUR) National Innovation Ecosystem grant ECS00000041-VITALITY-CUP: J97G22000170005 and B43C22000470005. This research was funded by Next Generation EU Programme: project PRIN-2022JWAF7Y and I-PHOQS Infrastructure [IR0000016, ID D2B8D520, CUP B53C22001750006]; project CNR-FOE-LENS-2023 and Horizon 2020 EU Programme project Laserlab-Europe n. 871124.

Appendix A. Supplementary data

Supplementary data to this article can be found online at https://doi.org/10.1016/j.foodhyd.2024.110863.

Data availability

Data will be made available on request.

References

Ahmed, Z., Beta, I. A., Mikhonin, A. V., & Asher, S. A. (2005). UV-resonance Raman thermal unfolding study of Trp-cage shows that it is not a simple two-state miniprotein. *Journal of the American Chemical Society, 127*(31), 10943–10950. https://doi.org/10.1021/ja050664e

Alfano, C., Fichou, Y., Huber, K., Weiss, M., Spruijt, E., Ebbinghaus, S., De Luca, G., Morando, M. A., Vetri, V., Temussi, P. A., & Pastore, A. (2024). Molecular crowding: The history and development of a Scientific paradigm. *Chemical Reviews, 124*(6), 3186–3219. https://doi.org/10.1021/acs.chemrev.3c00615. American Chemical Society.

Amirkhani, M., Taschin, A., Cucini, R., Bartolini, P., Leporini, D., & Torre, R. (2011). Polymer thermal and acoustic properties using heterodyne detected transient grating technique. *Journal of Polymer Science, Part B: Polymer Physics, 49*(9), 685–690. https://doi.org/10.1002/polb.22233

Anghel, L., Rogachev, A., Kuklin, A., & Erhan, R. V. (2019). β-Lactoglobulin associative interactions: A small-angle scattering study. *European Biophysics Journal, 48*(3), 285–295. https://doi.org/10.1007/s00249-019-01360-9

Asher, S. A., Ludwig, M., & Johnson, C. R. (1986). UV resonance Raman excitation profiles of the aromatic amino acids. *Journal of the American Chemical Society, 108* (2). https://pubs.acs.org/sharingguidelines.

Babcock, J. J., & Brancaleon, L. (2013). Bovine serum albumin oligomers in the E- and B-forms at low protein concentration and ionic strength. *International Journal of Biological Macromolecules, 53*, 42–53. https://doi.org/10.1016/j.ijbiomac.2012.10.030

Barbosa, L. R. S., Ortore, M. G., Spinozzi, F., Mariani, P., Bernstorff, S., & Itri, R. (2010). The importance of protein-protein interactions on the pH-induced conformational changes of bovine serum albumin: A small-angle x-ray scattering study. *Biophysical Journal, 98*(1), 147–157. https://doi.org/10.1016/j.bpj.2009.09.056

Cao, Y., & Mezzenga, R. (2019). Food protein amyloid fibrils: Origin, structure, formation, characterization, applications and health implications. In *Advances in colloid and interface science* (Vol. 269, pp. 334–356). Elsevier B.V. https://doi.org/10.1016/j.cis.2019.05.002

Catalini, S., Lutz-Bueno, V., Usuelli, M., Diener, M., Taschin, A., Bartolini, P., Foggi, P., Paolantoni, M., Mezzenga, R., & Torre, R. (2022). Multi-length scale structural investigation of lysozyme self-assembly. *iScience, 25*(7). https://doi.org/10.1016/j.isci.2022.104586

Catalini, S., Perinelli, D. R., Sassi, P., Comez, L., Palmieri, G. F., Morresi, A., Bonacucina, G., Foggi, P., Pucciarelli, S., & Paolantoni, M. (2021). Amyloid self-assembly of lysozyme in self-crowded conditions: The formation of a protein oligomer hydrogel. *Biomacromolecules, 22*(3), 1147–1158. https://doi.org/10.1021/acs.biomac.0c01652

Catalini, S., Taschin, A., Bartolini, P., Foggi, P., & Torre, R. (2019). Probing globular protein self-assembling dynamics by heterodyne transient grating experiments. *Applied Sciences, 9*(3). https://doi.org/10.3390/app9030405

Chi, Z., & Asher, S. A. (1998a). UV Raman determination of the environment and solvent exposure of Tyr and Trp residues. *Journal of Physical Chemistry B, 102*(47), 9595–9602. https://doi.org/10.1021/jp9828336

Chi, Z., & Asher, S. A. (1998b). UV Raman determination of the environment and solvent exposure of Tyr and Trp residues. *Journal of Physical Chemistry B, 102*(47), 9595–9602. https://doi.org/10.1021/jp9828336

Comez, L., Gentili, P. L., Paolantoni, M., Paciaroni, A., & Sassi, P. (2021). Heat-induced self-assembling of BSA at the isoelectric point. *International Journal of Biological Macromolecules, 177*, 40–47. https://doi.org/10.1016/j.ijbiomac.2021.02.112

Cucini, R., Taschin, A., Bartolini, P., & Torre, R. (2010a). Acoustic phenomena and hydrodynamic flow in a water filled nano-porous glass studied by transient grating spectroscopy. *Journal of Physics: Conference Series, 214*. https://doi.org/10.1088/1742-6596/214/1/012032

Cucini, R., Taschin, A., Bartolini, P., & Torre, R. (2010b). Acoustic, thermal and flow processes in a water filled nanoporous glass by time-resolved optical spectroscopy. *Journal of the Mechanics and Physics of Solids, 58*(9), 1302–1317. https://doi.org/10.1016/j.jmps.2010.06.002

Dave, A. C., Loveday, S. M., Anema, S. G., Loo, T. S., Norris, G. E., Jameson, G. B., & Singh, H. (2013). β-lactoglobulin self-assembly: Structural changes in early stages and disulfide bonding in fibrils. *Journal of Agricultural and Food Chemistry, 61*(32), 7817–7828. https://doi.org/10.1021/jf401084f

De Castro, R. J. S., Domingues, M. A. F., Ohara, A., Okuro, P. K., dos Santos, J. G., Brexó, R. P., & Sato, H. H. (2017). Whey protein as a key component in food systems: Physicochemical properties, production technologies and applications. *Food Structure, 14*, 17–29. https://doi.org/10.1016/j.foostr.2017.05.004

Dobson, C. M. (2004). Principles of protein folding, misfolding and aggregation. *Seminars in Cell & Developmental Biology, 15*(1), 3–16. https://doi.org/10.1016/j.semcdb.2003.12.008

Foley, J., Hill, S. E., Miti, T., Mulaj, M., Ciesla, M., Robeel, R., Raynes, R., Westerheide, S., & Muschol, M. (2013). Structural fingerprints and their evolution during oligomeric vs. oligomer-free amyloid fibril growth. *The Journal of Chemical Physics, 139*(12). https://doi.org/10.1063/1.4811343

Haider, R., Sartori, B., Radeticchio, A., Wolf, M., Zilio, S. D., Marmiroli, B., & Amenitsch, H. (2021). MDrop: A system for high-throughput small-angle X-ray scattering measurements of microlitre samples. *Journal of Applied Crystallography, 54*, 132–141. https://doi.org/10.1107/S1600576720014788

Herneke, A., Lendel, C., Johansson, D., Newson, W., Hedenqvist, M., Karkehabadi, S., Jonsson, D., & Langton, M. (2021). Protein nanofibrils for sustainable food-characterization and comparison of fibrils from a broad range of plant protein isolates. *Food Science and Technology, 1*(5), 854–864. https://doi.org/10.1021/acsfoodscitech.1c00034

Heyn, T. R., Garamus, V. M., Neumann, H. R., Uttinger, M. J., Guckeisen, T., Heuer, M., Selhuber-Unkel, C., Peukert, W., & Keppler, J. K. (2019). Influence of the polydispersity of pH 2 and pH 3.5 beta-lactoglobulin amyloid fibril solutions on analytical methods. *European Polymer Journal, 120*. https://doi.org/10.1016/j.eurpolymj.2019.08.038

Hoppenreijs, L. J. G., Fitzner, L., Ruhmlieb, T., Heyn, T. R., Schild, K., van der Goot, A. J., Boom, R. M., Steffen-Heins, A., Schwarz, K., & Keppler, J. K. (2022). Engineering amyloid and amyloid-like morphologies of β-lactoglobulin. *Food Hydrocolloids, 124*, Article 107301. https://doi.org/10.1016/j.foodhyd.2021.107301

Hughes, M. D. G., Hanson, B. S., Cussons, S., Mahmoudi, N., Brockwell, D. J., & Dougan, L. (2021). Control of nanoscale in situ protein unfolding defines network architecture and mechanics of protein hydrogels. *ACS Nano, 15*(7), 11296–11308. https://doi.org/10.1021/acsnano.1c00353

Ikeda, S., & Morris, V. J. (2002). Fine-stranded and particulate aggregates of heat-denatured whey proteins visualized by atomic force microscopy. *Biomacromolecules, 3*(2), 382–389. https://doi.org/10.1021/bm0156429

Iwashita, K., Handa, A., & Shiraki, K. (2017). Co-aggregation of ovalbumin and lysozyme. *Food Hydrocolloids, 67*, 206–215. https://doi.org/10.1016/j.foodhyd.2017.01.014

Jaeger, A., Ahern, N., Sahin, A. W., Nyhan, L., Mes, J. J., van der Aa, C., Vrasidas, I., & Arendt, E. K. (2024). Dynamic in-vitro system indicates good digestibility characteristics for novel upcycled plant protein; correlation to techno-functional properties. *Innovative Food Science and Emerging Technologies, 92*. https://doi.org/10.1016/j.ifset.2024.103571

Jansens, K. J. A., Rombouts, I., Grootaert, C., Brijs, K., Van Camp, J., Van der Meeren, P., Rousseau, F., Schymkowitz, J., & Delcour, J. A. (2019). Rational design of amyloid-like fibrillary structures for tailoring food protein techno-functionality and their potential health implications. *Comprehensive Reviews in Food Science and Food Safety, 18*(1), 84–105. https://doi.org/10.1111/1541-4337.12404

Kehoe, J. J., Morris, E. R., & Brodkorb, A. (2007). The influence of bovine serum albumin on β-lactoglobulin denaturation, aggregation and gelation. *Food Hydrocolloids, 21*(5–6), 747–755. https://doi.org/10.1016/j.foodhyd.2006.10.001

Kelly, S. M., Jess, T. J., & Price, N. C. (2005). How to study proteins by circular dichroism. *Biochimica et Biophysica Acta - Proteins and Proteomics, 1751*(2), 119–139. https://doi.org/10.1016/j.bbapap.2005.06.005

Khalesi, H., Sun, C., He, J., Lu, W., & Fang, Y. (2021). The role of amyloid fibrils in the modification of whey protein isolate gels with the form of stranded and particulate microstructures. *Food Research International, 140*. https://doi.org/10.1016/j.foodres.2020.109856

Kurouski, D., Duyne, P. Van, & Lednev, I. K. (2015). *Exploring the structure and formation mechanism of amyloid fibrils by Raman spectroscopy: A review*. https://doi.org/10.1039/c5an00342c

Kurouski, D., Lauro, W., & Lednev, I. K. (2010). Amyloid fibrils are alive: Spontaneous refolding from one polymorph to another. *Chemical Communications, 46*(24), 4249–4251. https://doi.org/10.1039/b926758a

Kurouski, D., Van Duyne, R. P., & Lednev, I. K. (2015). Exploring the structure and formation mechanism of amyloid fibrils by Raman spectroscopy: A review. *Analyst, 140*(15), 4967–4980. https://doi.org/10.1039/c5an00342c

Kurouski, D., Washington, J., Ozbil, M., Prabhakar, R., Shekhtman, A., & Lednev, I. K. (2012). Disulfide bridges remain intact while native insulin converts into amyloid fibrils. *PLoS One, 7*(6), 1–9. https://doi.org/10.1371/journal.pone.0036989

Lara, C., Adamcik, J., Jordens, S., & Mezzenga, R. (2011). General self-assembly mechanism converting hydrolyzed globular proteins into giant multistranded amyloid ribbons. *Biomacromolecules, 12*(5), 1868–1875. https://doi.org/10.1021/bm200216u

Laue, T. (2012). Proximity energies: A framework for understanding concentrated solutions. *Journal of Molecular Recognition, 25*(3), 165–173. https://doi.org/10.1002/jmr.2179

Lazidis, A., Hancocks, R. D., Spyropoulos, F., Kreuß, M., Berrocal, R., & Norton, I. T. (2016). Whey protein fluid gels for the stabilisation of foams. *Food Hydrocolloids, 53*, 209–217. https://doi.org/10.1016/j.foodhyd.2015.02.022

Liu, H., Liu, C., McClements, D. J., Xu, X., Bai, C., Sun, Q., Xu, F., & Dai, L. (2024). Reinforcement of heat-set whey protein gels using whey protein nanofibers: Impact of nanofiber morphology and pH values. *Food Hydrocolloids, 153*. https://doi.org/10.1016/j.foodhyd.2024.109954

López-Peña, I., Leigh, B. S., Schlamadinger, D. E., & Kim, J. E. (2015). Insights into protein structure and dynamics by ultraviolet and visible resonance Raman spectroscopy. *Biochemistry, 54*(31), 4770–4783. https://doi.org/10.1021/acs.biochem.5b00514

McClements, D. J. (2024). Composite hydrogels assembled from food-grade biopolymers: Fabrication, properties, and applications. *Advances in Colloid and Interface Science, 332*. https://doi.org/10.1016/j.cis.2024.103278

Mezzenga, R., & Fischer, P. (2013). The self-assembly, aggregation and phase transitions of food protein systems in one, two and three dimensions. *Reports on Progress in Physics, 76*(4). https://doi.org/10.1088/0034-4885/76/4/046601

Model, M. A., Hollembeak, J. E., & Kurokawa, M. (2021). Macromolecular crowding: A hidden link between cell volume and everything else. *Cellular Physiology and Biochemistry, 55*(S1), 25–40. https://doi.org/10.33594/000000319

Moitzi, C., Donato, L., Schmitt, C., Bovetto, L., Gillies, G., & Stradner, A. (2011). Structure of β-lactoglobulin microgels formed during heating as revealed by small-angle X-ray scattering and light scattering. *Food Hydrocolloids, 25*(7), 1766–1774. https://doi.org/10.1016/j.foodhyd.2011.03.020

Nicolai, T. (2019). Gelation of food protein-protein mixtures. *Advances in Colloid and Interface Science, 270*, 147–164. https://doi.org/10.1016/j.cis.2019.06.006

Qin, Y., Chen, X., Xu, F., Gu, C., Zhu, K., Zhang, Y., Wu, G., Wang, P., & Tan, L. (2023). Effects of hydroxylation at C3′ on the B ring and diglycosylation at C3 on the C ring on flavonols inhibition of α-glucosidase activity. *Food Chemistry, 406*. https://doi.org/10.1016/j.foodchem.2022.135057

Qin, Y., Zhang, Y., Chen, X., Xu, F., Zhu, K., Wang, P., & Zhang, Y. (2024). Synergistic effect of pectin and the flavanols mixture on in vitro starch digestion and the corresponding mechanism. *Food Hydrocolloids, 158*. https://doi.org/10.1016/j.foodhyd.2024.110554

Rossi, B., Bottari, C., Catalini, S., D'Amico, F., Gessini, A., & Masciovecchio, C. (2020). Synchrotron-based ultraviolet resonance Raman scattering for material science. *Molecular and Laser Spectroscopy*. https://doi.org/10.1016/b978-0-12-818870-5.00013-7

Rossi, B., Tortora, M., Catalini, S., & Gessini, A. (2022). Synchrotron-based UV resonance Raman spectroscopy for polymer characterization. *Spectroscopic techniques for polymer characterization: Methods, instrumentation* (pp. 183–225). Applications. https://doi.org/10.1002/9783527830312.ch7

Schlamadinger, D. E., Gable, J. E., & Kim, J. E. (2009). Hydrogen bonding and solvent polarity markers in the UV resonance Raman spectrum of tryptophan: Application to membrane proteins. *Journal of Physical Chemistry B, 113*(44), 14769–14778. https://doi.org/10.1021/jp905473y

Shashilov, V., Xu, M., Ermolenkov, V. V., Fredriksen, L., & Lednev, I. K. (2007). Probing a fibrillation nucleus directly by deep ultraviolet Raman spectroscopy. *Journal of the American Chemical Society, 129*(22), 6972–6973. https://doi.org/10.1021/ja070038c

Siposova, K., Petrenko, V. I., Garcarova, I., Sedlakova, D., Almásy, L., Kyzyma, O. A., Kriechbaum, M., & Musatov, A. (2022). The intriguing dose-dependent effect of selected amphiphilic compounds on insulin amyloid aggregation: Focus on a cholesterol-based detergent. *Chobimalt. Frontiers in Molecular Biosciences, 9*. https://doi.org/10.3389/fmolb.2022.955282

Taschin, A., Bartolini, P., Eramo, R., & Torre, R. (2006). Supercooled water relaxation dynamics probed with heterodyne transient grating experiments. *Physical Review E - Statistical, Nonlinear and Soft Matter Physics*. https://doi.org/10.1103/PhysRevE.74.031502

Tomczyńska-Mleko, M., Kamysz, E., Sikorska, E., Puchalski, C., Mleko, S., Ozimek, L., Kowaluk, G., Gustaw, W., & Wesołowska-Trojanowska, M. (2014). Changes of secondary structure and surface tension of whey protein isolate dispersions upon ph and temperature. *Czech Journal of Food Sciences, 32*(1), 82–89. https://doi.org/10.17221/326/2012-CJFS

Varga, N., Hornok, V., Sebok, D., & Dékány, I. (2016). Comprehensive study on the structure of the BSA from extended-to aged form in wide (2-12) pH range. *International Journal of Biological Macromolecules, 88*, 51–58. https://doi.org/10.1016/j.ijbiomac.2016.03.030

Venturi, S., Rossi, B., Tortora, M., Torre, R., Lapini, A., Foggi, P., Paolantoni, M., & Catalini, S. (2023). Amyloidogenic and non-amyloidogenic molten globule conformation of β-lactoglobulin in self-crowded regime. *International Journal of Biological Macromolecules, 242*. https://doi.org/10.1016/j.ijbiomac.2023.124621

Xu, M., Ermolenkov, V. V., Uversky, V. N., & Lednev, I. K. (2008). Hen egg white lysozyme fibrillation: A deep-UV resonance Raman spectroscopic study. *Journal of Biophotonics, 1*(3), 215–229. https://doi.org/10.1002/jbio.200710013

Xu, D., Zhou, J., Soon, W. L., Kutzli, I., Molière, A., Diedrich, S., Radiom, M., Handschin, S., Li, B., Li, L., Sturla, S. J., Ewald, C. Y., & Mezzenga, R. (2023). Food amyloid fibrils are safe nutrition ingredients based on in-vitro and in-vivo assessment. *Nature Communications, 14*(1). https://doi.org/10.1038/s41467-023-42486-x

Yan, H., Frielinghaus, H., Nykanen, A., Ruokolainen, J., Saiani, A., & Miller, A. F. (2008). Thermoreversible lysozyme hydrogels: Properties and an insight into the gelation pathway. *Soft Matter, 4*(6), 1313–1325. https://doi.org/10.1039/b716966c

Zhang, J., Li, M., Lv, Y., Guo, S., & Yang, B. (2023). Protein aggregation impacts in vitro protein digestibility, peptide profiling and potential bioactive peptides of soymilk and dry-heated soybeans. *LWT, 182*. https://doi.org/10.1016/j.lwt.2023.114857

Zhao, K., Zhang, S., Piao, C., Xu, F., Zhang, Y., Wang, X., Zhang, J., Zhao, C., You, S. G., & Zhang, Y. (2024). Investigation of the formation mechanism of the pepper starch-piperine complex. *International Journal of Biological Macromolecules, 268*. https://doi.org/10.1016/j.ijbiomac.2024.131777

Zhu, Z., Pius Bassey, A., Cao, Y., Ma, Y., Huang, M., & Yang, H. (2022). Food protein aggregation and its application. *Food Research International, 160*. https://doi.org/10.1016/j.foodres.2022.111725